nature nanotechnology

LETTERS

PUBLISHED ONLINE: 12 OCTOBER 2014 | DOI: 10.1038/NNANO.2014.216

An addressable quantum dot qubit with fault-tolerant control-fidelity

M. Veldhorst[1]*, J. C. C. Hwang[1], C. H. Yang[1], A. W. Leenstra[2], B. de Ronde[2], J. P. Dehollain[1], J. T. Muhonen[1], F. E. Hudson[1], K. M. Itoh[3], A. Morello[1] and A. S. Dzurak[1]*

Exciting progress towards spin-based quantum computing[1,2] has recently been made with qubits realized using nitrogen-vacancy centres in diamond and phosphorus atoms in silicon[3]. For example, long coherence times were made possible by the presence of spin-free isotopes of carbon[4] and silicon[5]. However, despite promising single-atom nanotechnologies[6], there remain substantial challenges in coupling such qubits and addressing them individually. Conversely, lithographically defined quantum dots have an exchange coupling that can be precisely engineered[1], but strong coupling to noise has severely limited their dephasing times and control fidelities. Here, we combine the best aspects of both spin qubit schemes and demonstrate a gate-addressable quantum dot qubit in isotopically engineered silicon with a control fidelity of 99.6%, obtained via Clifford-based randomized benchmarking and consistent with that required for fault-tolerant quantum computing[7,8]. This qubit has dephasing time $T_2^* = 120$ μs and coherence time $T_2 = 28$ ms, both orders of magnitude larger than in other types of semiconductor qubit. By gate-voltage-tuning the electron g^*-factor we can Stark shift the electron spin resonance frequency by more than 3,000 times the 2.4 kHz electron spin resonance linewidth, providing a direct route to large-scale arrays of addressable high-fidelity qubits that are compatible with existing manufacturing technologies.

The seminal work by Loss and DiVincenzo[1] to encode quantum information using the spin states of semiconductor quantum dots generated great excitement, as it fulfilled what were then understood to be the key criteria[2] for quantum computation, and led to the realization of 2-qubit operations such as $\sqrt{\text{SWAP}}$[9,10] and CPHASE[11]. However, the limited lifetime and associated fidelity of the quantum state are a significant hurdle for the semiconductor quantum dot qubits realized thus far. A dephasing time of up to $T_2^* = 37$ ns (ref. 12), improved to $T_2^* = 94$ ns (ref. 13) using nuclear spin bath control, has been recorded for quantum dot spin qubits in GaAs/AlGaAs. A longer $T_2^* = 360$ ns has been achieved using Si/SiGe quantum dots[14]. The main strategy to improve these times has involved applying the pulse sequences developed for bulk magnetic resonance, and we can specify a T_2 according to the applied pulse sequence. Using a Hahn echo sequence the coherence time of GaAs-based qubits has been extended to $T_2^{\text{H}} = 440$ ns (ref. 12), with $T_2^{\text{H}} = 30$ μs achieved via pulse optimization[15], while the use of a Carr–Purcell–Meiboom–Gill (CPMG) pulse sequence has enabled $T_2^{\text{CPMG}} = 200$ μs (ref. 15). Here, by realizing a quantum dot qubit in isotopically enriched silicon (^{28}Si), we remove the dephasing effect of the nuclear spin bath present in these previous studies, and show that all of the above coherence times can be improved by orders of magnitude. These long coherence times, in particular the dephasing time T_2^*, lead to low control error rates and the high fidelities that will be required for large-scale, fault-tolerant quantum computing[7,8].

In contrast to quantum dots, electron spin qubits localized on atoms or defects have been realized in almost spin-free environments, showing coherence times approaching[4] and even exceeding seconds[5]. However, coupling multiple qubits and addressing them individually will be highly non-trivial for these systems, although these are key requirements for scalable quantum computation. A recent proposal has suggested that addressability might be possible using atom clusters[16], but here we demonstrate a qubit that can be addressed and tuned via a simple gate voltage. Strong spin–orbit coupling in InAs has enabled qubits to be realized in double quantum dots with distinct electron g-factors[17], but in silicon the spin–orbit coupling is much smaller[18]. Despite this, the highly tunable quantum dot presented here allows us to vary the internal electric field by as much as 3 MV m^{-1}, resulting in a Stark shift that can tune the electron spin resonance (ESR) frequency by >8 MHz. Also, the long T_2^* available in isotopically enriched silicon results in a narrow ESR linewidth of 2.4 kHz. Consequently, we can tune the qubit operation frequency by more than 3,000 times the minimum linewidth. These results, together with the inherent scalability of gated quantum dot qubits, open the possibility for large-scale and gate-voltage-addressable qubit systems. Such systems can utilize existing technology for the manufacture of the metal–oxide–semiconductor field-effect transistors (MOSFETs) that constitute today's computer processors.

Figure 1a,b presents a scanning electron microscope (SEM) image and a schematic design of the device, fabricated using a multi-level gate-stack silicon MOS technology[19]. The device was fabricated on an epitaxially grown, isotopically purified ^{28}Si epilayer with a residual concentration of ^{29}Si at 800 ppm (ref. 20). An on-chip transmission line[21] was incorporated to manipulate the spin states of the dot using ESR pulses. The single electron transistor (SET) adjacent to the quantum dot structure was used as a sensor to monitor the electron occupancy within the quantum dot, as reported previously[22]. The stability diagram for the quantum dot (Fig. 1c) was obtained by gate pulsing and combining charge sensing with a feedback loop to retain maximum sensitivity. The depletion of the last electron in the dot is observed in Fig. 1c, with no further charge transitions for $V_{\text{G4}} < 1.6$ V. Figure 1d presents typical examples of single-shot spin readout measurements for the last electron, using spin-to-charge conversion[23]. Further details of the spin readout measurements are provided in Supplementary Section 2. All qubit spin statistics were obtained using this method.

To control and read the qubit state we make use of a two-level pulse sequence, as shown in Fig. 2a. The tunnel coupling

[1]Centre for Quantum Computation and Communication Technology, School of Electrical Engineering and Telecommunications, The University of New South Wales, Sydney, New South Wales 2052, Australia, [2]University of Twente, PO Box 217, 7500 AE Enschede, The Netherlands, [3]School of Fundamental Science and Technology, Keio University, 3-14-1 Hiyoshi, Kohoku-ku, Yokohama 223-8522, Japan. *e-mail: m.veldhorst@unsw.edu.au; a.dzurak@unsw.edu.au

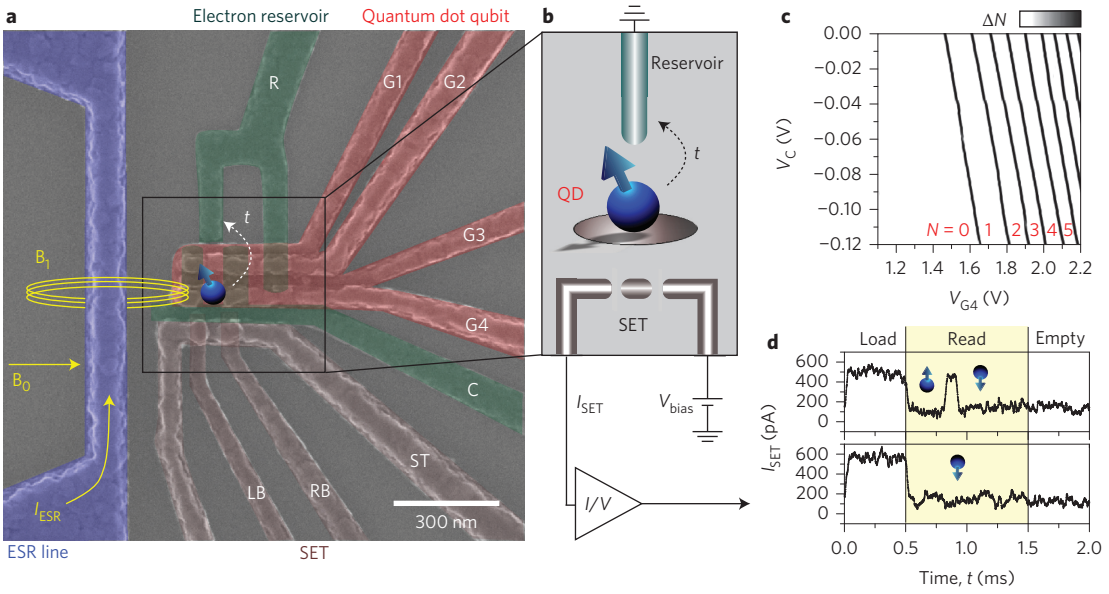

Figure 1 | Silicon quantum dot qubit with single electron transistor (SET) readout and on-chip microwave spin control. a,**b**, False-coloured SEM image (**a**) and schematic diagram (**b**) of the device. The quantum dot structure (labels C and G) can be operated as a single or double quantum dot by appropriate biasing of gate electrodes G1 to G4. Confinement gate C runs under gates G2 to G4 and confines the quantum dot on all sides except on the reservoir side. Here, we operate the system in the single quantum dot mode, with the dot defined under G4 and tunnel-coupled via G3 to reservoir R. This provides maximum flexibility and the largest readout signal, as the dot is then closest to the SET. ST, SET top gate; LB, left barrier gate; RB, right barrier gate. **c**, Charge stability diagram. The SET is used as a charge detector, and a feedback loop is included to obtain maximum sensitivity. A square pulse of 40 mV peak-to-peak at 174 Hz is applied to G4. Grey scale indicates the excess electron occupancy (ΔN) in the dot for each charge addition. The absence of any intermediate colour is a confirmation of the high fidelity. **d**, By changing the voltage on G4, we can load and empty the quantum dot, performing spin readout in a single-shot measurement via energy-selective tunnelling. All measurements were performed in a dilution refrigerator with a base temperature of $T \approx 50$ mK and a d.c. magnetic field of $B_0 = 1.4$ T.

between dot and reservoir is tuned using the barrier gate G3 to yield a tunnel time $t \approx 100$ µs during the read phase. There is almost no coupling in the control phase because the Zeeman-split spin states are plunged well below the Fermi level in the reservoir. We apply microwave pulses to the on-chip transmission line to create an a.c. magnetic field B_1, which drives transitions between the spin-down $|\downarrow\rangle$ and spin-up $|\uparrow\rangle$ states of the quantum dot[24]. When $B \approx 1.400$ T, we find the resonance frequency $\nu_0 = (g^*\mu_B/h)$ $B_{dc} \approx 39.1408$ GHz, resulting in $g^* \approx 1.998$. The qubit demonstrates coherent oscillations that coincide with $f_\uparrow = A \times \Omega^2/\Omega_R^2 \sin^2(\Omega_R\tau/2)$, describing a qubit without decay and a visibility of $A = 0.7$. We note that device stability limits the size of the data set that can be taken, so no decay was observed over the 30 µs shown in Fig. 2b. The Rabi decay time is ~380 µs, as shown in Supplementary Fig. 4 using a Carr-Purcell sequence. Figure 2b shows sinusoidal Rabi oscillations obtained by varying the pulse length τ_p, and Fig. 2c shows the oscillations while varying frequency ν_{ESR}. Confirmation that these are Rabi oscillations follows from the dependence $f_{Rabi} \propto B_1 \propto P_{ESR}^{1/2}$ (Fig. 2c, inset), where P_{ESR} is the applied microwave source power, and also from the increase in Rabi frequency for non-zero detuning frequency (Fig. 2d).

When the detuning frequency is non-zero, coherent oscillations known as Ramsey fringes arise when the spin is pointing in the x–y plane of the Bloch sphere. We detect these fringes by applying two $\pi/2$ pulses separated by a delay time τ, followed by readout of the spin state. The resulting oscillations are shown in Fig. 3a, from which we extract a characteristic decay time of $T_2^* = 120$ µs. The corresponding linewidth $1/\pi T_2^* = 2.6$ kHz is close to the smallest measured ESR peak width $\Delta\nu = 2.4 \pm 0.2$ kHz measured at $P_{ESR} = -20$ dBm (Supplementary Fig. 2). Slow environmental changes between individual single-shot readout events are one of the main factors leading to the decay of the Ramsey coherence fringes. To remove the effects of this noise we applied a Hahn-echo technique, where a π_x pulse is applied exactly between two $\pi_x/2$ pulses (Fig. 3b). From this we measure a spin coherence time of $T_2^H = 1.2$ ms. The Hahn-echo amplitude decays with an exponent $\eta = 2.2$, indicating that the dominant source of decoherence is $1/f$ noise. We can further increase the coherence time by applying a CPMG sequence, where a series of π_y pulses are applied to refocus the signal. Figure 3c shows an echo decay obtained by applying 500 π_y pulses, with a resulting coherence time of $T_2^{CPMG} = 28$ ms.

We now turn to the qubit fidelities (see Supplementary Section 4 for full details). The measurement fidelity $F_M = 92\%$ and initialization fidelity $F_I = 95\%$ are primarily limited by thermal broadening in the electron reservoir. The broadening leads to a small fraction of unintended random tunnelling events between the reservoir and dot, corresponding to initialization and readout errors[21], thus limiting the visibility of the Rabi oscillations shown in Fig. 2, for example. However, during the control phase the electron level is plunged deep below the Fermi level in the reservoir, to avoid such errors.

We have characterized the control fidelity of the qubit via randomized benchmarking[25] on Clifford gates (Fig. 4). In this protocol, the fidelity of an individual Clifford gate is obtained by interleaving it with random Clifford gates and measuring the decay with increasing sequence length. The protocol ends with a final random recovery Clifford, such that the outcome is either spin up or spin down. A reference sequence without interleaved gates is performed to observe the decay due to the random Cliffords. By analysing the data we find an average control fidelity of $F_C = 99.59\%$, with all gates having an error rate below the 1% tolerance requirement for quantum error correction using surface codes[8]. When the operation time of the qubit is an appreciable fraction of T_2^*, dephasing can result in a non-exponential decay (Supplementary Section 4). This could explain the slightly non-exponential decay we observe in Fig. 4, and opens the possibility to further increase the fidelity by making use of composite and

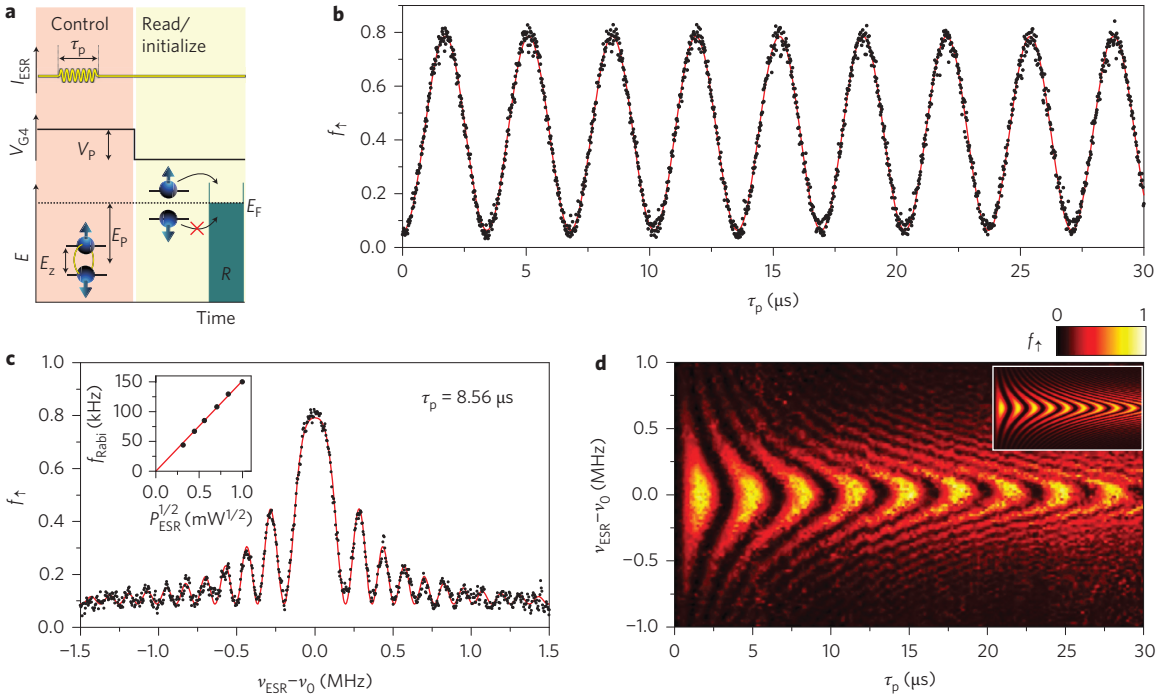

Figure 2 | Electron spin resonance (ESR) and Rabi oscillations. a, Pulsing scheme for qubit control and readout. The Zeeman-split electron spin levels are plunged to energy E_P using gate G4, and ESR pulses are applied to rotate the spin on the Bloch sphere. Subsequently, the electron levels are increased to straddle the Fermi energy of reservoir R, enabling spin readout. After readout the qubit is automatically initialized in the spin-down state. **b**, Electron spin-up fraction $f_\uparrow$ as a function of the microwave burst duration τ_p, with $P_{ESR} = 5$ dBm. **c**, Electron spin-up fraction $f_\uparrow$ as a function of ESR frequency around the resonance frequency, $\nu_0 = 39.1408$ GHz, with $\tau_p = 8.56$ μs (corresponding to the peak of the third Rabi oscillation). **d**, Colour map of measured spin-up fraction $f_\uparrow$, showing Rabi oscillations as a function of τ_p for different microwave detuning frequencies. Inset: Corresponding calculated Rabi oscillations. All data in **b**–**d** are fitted by assuming no decay in time and using $f_\uparrow = A \times \Omega^2/\Omega_R^2 \sin^2(\Omega_R\tau/2)$, where Ω and Ω_R are the Rabi and total Rabi frequency, respectively. The visibility $A = 0.7$ is determined from the experimental data.

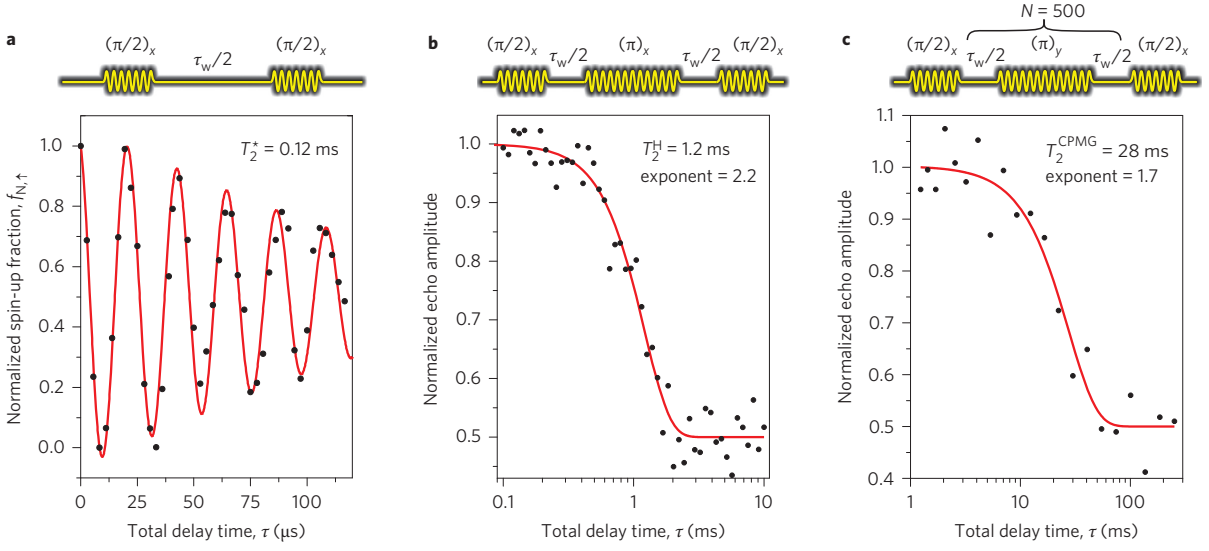

Figure 3 | Qubit coherence. The spin state statistics are normalized with respect to the visibility to account for fluctuations between different measurements. **a**, By varying the delay time τ_w between two $\pi_x/2$ pulses (see schematic, top), Ramsey oscillations arise in the spin-up fraction $f_\uparrow$. Fitting the decay with $f_{N,\uparrow} = e^{-[\tau/T_2^*]^\alpha}$, with $\alpha = 1.3$, we deduce a dephasing time $T_2^* = 120$ μs. **b**, A Hahn-echo pulse sequence incorporates an additional π-pulse (schematic, top) and compensates for slow drifts in the environment. The resulting spin-up fraction $f_\uparrow$ decay gives the spin coherence time $T_2^H = 1.2$ ms. **c**, By applying a CPMG pulse sequence (schematic, top) we can further enhance the coherence time, giving $T_2^{CPMG} = 28$ ms.

shaped pulse sequences that correct for dephasing, as routinely used in NMR experiments.

The vertical electric field F_z in our quantum dot can be tuned over a large range by increasing the voltage on G4, while reducing the voltage on C to maintain an electron occupancy of $N = 1$. Recent experiments on silicon dots have observed an anticrossing of the spin and valley states (Fig. 5a, inset) due to spin–orbit coupling, which occurs in a small energy window of neV to μeV,

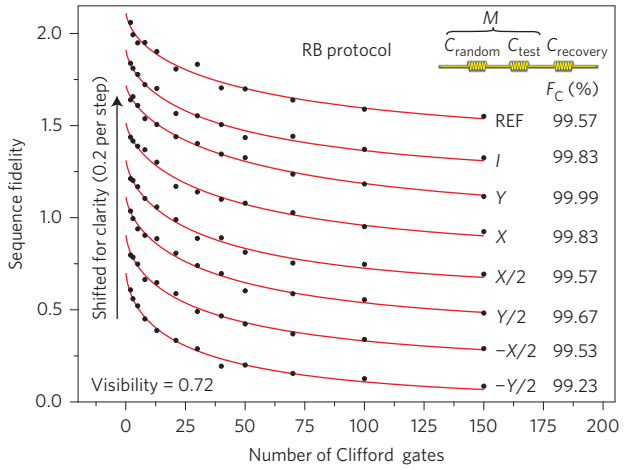

Figure 4 | Control fidelity analysis via randomized benchmarking of Clifford gates. The performance of each Clifford gate is tested by interleaving them with random Clifford gates. From the decay we infer an average fidelity of 99.59%, above the threshold required for quantum error correction using surface codes[8]. The sequence fidelity decays over more than 150 pulses, where M is the number of Clifford gates applied. A π-pulse of 1.6 μs and a waiting time of 500 ns between consecutive gates have been used. The data are vertically shifted by 0.2 per step and the visibility of all data is 0.72, limited by readout and initialization errors. Further details are provided in Supplementary Section 4.

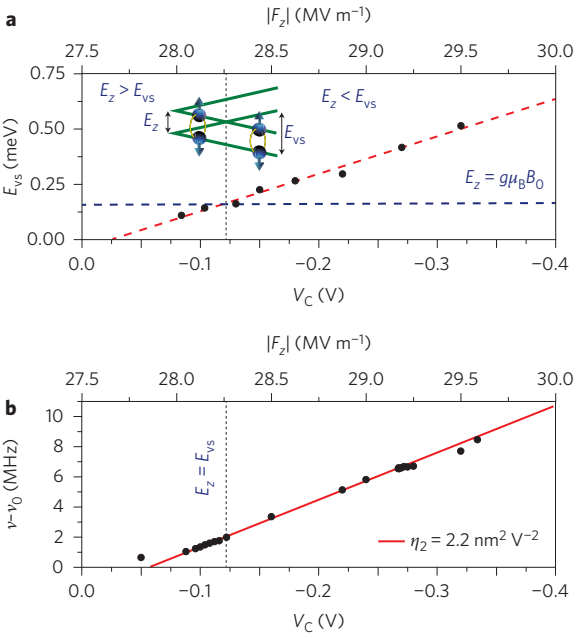

Figure 5 | Gate-voltage tunability of the qubit operation frequency and of the valley splitting. a, Measured valley splitting E_{vs}, obtained using the method of Yang and co-authors[26], as a function of the confinement gate potential V_C. Inset: Electron spin states for the two-valley system, with an anticrossing when the Zeeman energy $E_z = E_{vs}$. **b**, Measured qubit resonance frequency as a function of V_C, due to a small but finite Stark shift. The red line is a fit using $g(|F_z|)/g(0) - 1 = \eta_2|F_z|^2$, where $\eta_2 = 2.2$ nm^2 V^{-2}. The vertical electric field F_z (top axis) is calculated from the gate voltages using the numerical simulation of Yang and co-authors[26].

depending on the interface roughness[26,27]. Using a recently developed 'hot-spot' spin relaxation technique[26] we have measured (Supplementary Fig. 5) the magnitude of the valley splitting E_{vs} as a function of gate voltage (Fig. 5a) and find a linear dependence of E_{vs} upon F_z that differs by only 12% from a device reported previously[26].

The same internal electric field that we use to tune the valley splitting can also be used to tune the qubit resonance frequency by more than 8 MHz (Fig. 5b and Supplementary Information), corresponding to more than 3,000 times the minimum observed ESR linewidth. This tunability, which is remarkable for a system with these long coherence times, provides encouraging prospects for scalability. We can operate our device in regimes both above and below the spin-valley anticrossing with no discernible impact on the ESR frequency dependence with F_z, demonstrating a gate-addressable and high-fidelity qubit well away from the valley anti-crossing point, where the relaxation time dramatically drops[26]. The electric field creates a Stark shift of the electron g^*-factor due to the small but finite spin–orbit coupling. Tight binding simulations[18] and measurements on donors in silicon[28] indicate a quadratic Stark shift in g^*. By fitting our data we find a quadratic Stark coefficient of $\eta_2 = 2.2$ nm^2 V^{-2}, comparable to that calculated by Rahman and co-authors[18]. This Stark shift also opens a new channel for decoherence by electrical noise. Recently[29], a longer T_2^{CPMG} for a phosphorus donor qubit in ^{28}Si has been observed, possibly consistent with a smaller Stark shift in that case.

The results presented here demonstrate that a single electron spin confined to a quantum dot in isotopically purified silicon can serve as a robust qubit platform for solid-state quantum computing. We have demonstrated long qubit coherence times, high fidelity control over the qubit and the ability to individually address qubits via electrostatic gate-voltage control, meeting key criteria for quantum computation[2]. The relevant coherence times (T_2^*, T_2^H and T_2^{CPMG}) of our system exceed by two orders of magnitude the times of previous quantum dot qubits[14,15], while the fastest measured Rabi period of 400 ns combined with our $T_2^{CPMG} = 28$ ms enables more than 10^5 computational operations within the qubit coherence time. In a recent experiment[29] on a phosphorus donor qubit in ^{28}Si, comparable coherence times are observed. Based on noise spectroscopy measurements[29], the superconducting magnet is put forward as a viable candidate to cause the low-frequency noise, while Johnson–Nyquist thermal noise delivered via the on-chip ESR line is proposed as the source for the high-frequency noise. Further experiments are required to confirm whether these are the decoherence mechanisms in the present qubit and to reveal whether it is possible to increase coherence times even further.

Faster qubit operations could be achieved by operating pairs of quantum dots as singlet–triplet qubits[9], with the potential to further increase the number of coherent operations. Such singlet–triplet qubits could not rely on a magnetic field gradient from lattice nuclear spins, as these are absent in isotopically enriched silicon; however, a field gradient could be realized via an on-chip nanomagnet. The voltage-tunable Stark shift demonstrated here could also be exploited to create different effective g^*-factors for the individual dots.

Direct gate addressability opens the prospect for many qubits to be integrated on a single chip, with global a.c. magnetic fields applied via a cavity or on-chip transmission lines to realize single qubit operations. Two-qubit operations could then be achieved, for example, via gate-controlled exchange coupling between pairs of quantum dots. A recent model, applicable to our qubit system, predicts that 2-qubit gate operations with high fidelities are also possible[30]. Taken together with the high control fidelities demonstrated for our 1-qubit gate, this now places quantum dot spin qubits as a viable candidate for fault-tolerant quantum computing. While scaling qubits involves complex wiring and will be a formidable task, one control line per qubit could be sufficient for the platform presented here. A confinement potential could be realized with one gate designed as a large grid, and one top gate for each qubit for

addressing and controlling the exchange coupling to the other qubits. Finally, we note that the device structure used here can be modified to use poly-silicon gate electrodes and the standard complementary metal–oxide–semiconductor (CMOS) manufacturing technologies that are currently used to fabricate more than one billion transistors on a single chip.

Received 27 February 2014; accepted 28 August 2014; published online 12 October 2014

References

1. Loss, D. & DiVincenzo, D. P. Quantum computation with quantum dots. *Phys. Rev. A* **57,** 120–126 (1998).
2. DiVincenzo, D. P. The physical implementation of quantum computation. *Fortschr. Phys.* **48,** 771–783 (2000).
3. Awschalom, D. D., Bassett, L. C., Dzurak, A. S., Hu, E. L. & Petta, J. R. Quantum spintronics: engineering and manipulating atom-like spins in semiconductors. *Science* **339,** 1174–1179 (2012).
4. Bar-Gill, N., Pham, L. M., Jarmola, A., Budker, D. & Walsworth, R. L. Solid-state electronic spin coherence time approaching one second. *Nature Commun.* **4,** 1743 (2013).
5. Tyryshkin, A. M. *et al.* Electron spin coherence exceeding seconds in high-purity silicon. *Nature Mater* **11,** 143–147 (2012).
6. Fuechsle, M. *et al.* A single-atom transistor. *Nature Nanotech.* **7,** 242–246 (2012).
7. Knill, E. Quantum computing with realistically noisy devices. *Nature* **434,** 39–44 (2005).
8. Fowler, A., Marlantoni, M., Martinis, J. M. & Cleland, A. N. Surface codes: towards practical large-scale quantum computation. *Phys. Rev. A* **86,** 1–48 (2012).
9. Petta, J. R. *et al.* Coherent manipulation of coupled electron spins in semiconductor quantum dots. *Science* **309,** 2180–2184 (2005).
10. Nowack, K. C. *et al.* Single-shot correlations and two-qubit gate of solid-state spins. *Science* **333,** 1269–1272 (2011).
11. Shulman, M. D. *et al.* Demonstration of entanglement of electrostatically coupled singlet–triplet qubits. *Science* **336,** 202–205 (2012).
12. Koppens, F. H. L., Nowack, K. C. & Vandersypen, L. M. K. Spin echo of a single electron spin in a quantum dot. *Phys. Rev. Lett.* **100,** 236802 (2008).
13. Bluhm, H., Foletti, S., Mahalu, D., Umansky, V. & Yacoby, A. Enhancing the coherence of a spin qubit by operating it as a feedback loop that controls its nuclear spin bath. *Phys. Rev. Lett.* **105,** 216803 (2010).
14. Maune, B. M. *et al.* Coherent singlet–triplet oscillations in a silicon-based double quantum dot. *Nature* **481,** 344–347 (2012).
15. Bluhm, H. *et al.* Dephasing time of GaAs electron–spin qubits coupled to a nuclear bath exceeding 200 μs. *Nature Phys.* **7,** 109–113 (2011).
16. Büch, H., Mahapatra, S., Rahman, R., Morello, A. & Simmons, M. Y. Spin readout and addressability of phosphorus-donor clusters in silicon. *Nature Commun.* **4,** 2017 (2013).
17. Nadj-Perge, S., Frolov, S. M., Bakkers, E. P. A. M. & Kouwenhoven, L. P. Spin–orbit qubit in a semiconductor nanowire. *Nature* **468,** 1084–1087 (2010).
18. Rahman, R. *et al.* Gate-induced *g*-factor control and dimensional transition for donors in multivalley semiconductors. *Phys. Rev. B* **80,** 155301 (2009).
19. Angus, S. J., Ferguson, A. J., Dzurak, A. S. & Clark, R. G. Gate-defined quantum dots in intrinsic silicon. *Nano Lett.* **7,** 2051–2055 (2007).
20. Fukatsu, S. *et al.* Effect of the Si/SiO_2 interface on self-diffusion of Si in semiconductor-grade SiO_2. *Appl. Phys. Lett.* **83,** 3897–3899 (2003).
21. Pla, J. J. *et al.* A single-atom electron spin qubit in silicon. *Nature* **489,** 541–545 (2012).
22. Yang, C. H., Lim, W. H., Zwanenburg, F. A. & Dzurak, A. S. Dynamically controlled charge sensing of a few-electron silicon quantum dot. *AIP Adv.* **1,** 042111 (2011).
23. Elzerman, J. M. *et al.* Single-shot read-out of an individual electron spin in a quantum dot. *Nature* **430,** 431–435 (2004).
24. Koppens, F. H. L. *et al.* Driven coherent oscillations of a single electron spin in a quantum dot. *Nature* **442,** 766–771 (2006).
25. Knill, E. *et al.* Randomized benchmarking of quantum gates. *Phys. Rev. A* **77,** 012307 (2008).
26. Yang, C. H. *et al.* Spin-valley lifetimes in a silicon quantum dot with tunable valley splitting. *Nature Commun.* **4,** 2069 (2013).
27. Hao, X., Ruskov, R., Xiao, M., Tahan, C. & Jian, H. W. Electron spin resonance and spin-valley physics in a silicon double quantum dot. *Nature Commun.* **5,** 3860 (2014).
28. Bradbury, F. R. *et al.* Stark tuning of donor electron spins in silicon. *Phys. Rev. Lett.* **97,** 176404 (2006).
29. Muhonen, J. T. *et al.* Storing quantum information for 30 seconds in a nanoelectronic device. Preprint at http://arXiv.org/abs/1402.7140 (2014).
30. Kalra, R., Laucht, A., Hill, C. D. & Morello, A. Robust two-qubit gates for donors in silicon controlled by hyperfine interactions. *Phys. Rev. X* **4,** 021044 (2014).

Acknowledgements

The authors thank D. J. Reilly and J. R. Petta for discussions. The authors acknowledge support from the Australian Research Council (CE11E0096), the US Army Research Office (W911NF-13-1-0024) and the NSW Node of the Australian National Fabrication Facility. M.V. acknowledges support from the Netherlands Organization for Scientific Research (NWO) through a Rubicon Grant. The work at Keio has been supported in part by FIRST, the Core-to-Core Program by JSPS, and the Grant-in-Aid for Scientific Research and Project for Developing Innovation Systems by MEXT.

Author contributions

M.V., J.C.C.H., C.H.Y., A.W.L., B.R., J.P.D. and J.T.M. performed the experiments. M.V. and F.E.H. fabricated the devices. K.M.I. prepared and supplied the ^{28}Si epilayer wafer. M.V., C.H.Y., A.M. and A.S.D. designed the experiments and analysed the results. M.V. and A.S.D. wrote the manuscript, with input from all authors.

Additional information

Supplementary information is available in the online version of the paper. Reprints and permissions information is available online at www.nature.com/reprints. Correspondence and requests for materials should be addressed to M.V. and A.S.D.

Competing financial interests

The authors declare no competing financial interests.